Available online at www.sciencedirect.com
SCIENCE DIRECT®
Polymer 45 (2004) 1063–1071
polymer
www.elsevier.com/locate/polymer

Molecular modeling of cellulose in amorphous state. Part I: model building and plastic deformation study

Wei Chen[a,*,1], Gary C. Lickfield[a], Charles Q. Yang[b]

[a]School of Materials Science and Engineering, Clemson University, Clemson, SC 29634, USA
[b]Department of Textiles, Merchandising and Interiors, The University of Georgia, Athens, GA 30602-3622, USA

Received 7 April 2003; received in revised form 13 November 2003; accepted 13 November 2003

Abstract

Molecular modeling was utilized to provide insight into the yielding behavior and poor recovery from applied strain for cellulose. Amorphous cellulose models were successfully built and examined with the use of force field pcff_300_1.01. High-temperature molecular dynamics, followed by minimization, was used to generate relaxed structures for amorphous cellulose. Properties related to inter-molecular interactions were calculated for these models and found to be comparable with literature values. The observed yielding for these models, which occurred at approximately 7–8% strain, was found to be due to the disruption of hydrogen bonds between cellulose chain segments. New hydrogen bonds were formed in extension but only 1/3 of these were broken during recovery. These newly formed hydrogen bonds were found to hold the cellulose chain segments in the new positions thus resulting in poor deformation recovery.

Keywords: Molecular modeling; Cellulose; Hydrogen bonding

1. Introduction

It has been known for many years that the loss in mechanical properties of cellulose due to durable-press treatments can be severe. As a reactant, cellulose, as with most polymers, is limited in its accessibility by the physical restraints of the polymer morphology. The amorphous portion of cellulose is much more open and accessible than is the crystalline portion and, as such, crosslinking reactions occur mainly in these amorphous regions. Therefore, it is the properties of the amorphous portion which are influenced by durable-press treatments. It has been reported that almost one-third of the anhydroglucose units in the amorphous regions are bound by crosslinks at a 5.1% resin add-on [1]. With such an extent of chemical modification, it is not surprising that crosslinking also results in the loss of mechanical properties such as tensile strength, tear strength and abrasion resistance, resulting in reduced wear behavior of cellulose fabrics. This problem has plagued the textile industry and consumers for decades and considerable resources and efforts have been employed toward its resolution [2–8]. One of the goals of this research is to develop a molecular level of understanding of this phenomenon. Current molecular modeling techniques are suitable to provide the necessary tools to perform such an investigation.

The use of molecular modeling in research on cellulose structure can be traced back to the early 1980s. Since that time, molecular modeling has been used to help interpret X-ray diffraction data for cellulose crystals and to aid in understanding the structures of cellulose I and cellulose II [9,10]. Molecular modeling has also been used to study the structure-property relationships of a variety of amorphous polymers. Since the development by Theodorou and Suter [11] of a molecular modeling technique to generate models of a well-relaxed amorphous polypropylene, there have been numerous publications concerning molecular modeling of amorphous polymers [12–17]. However, little molecular modeling research has been done on the amorphous portion of cellulose, which is the focus of this research.

This paper presents the initial research work towards understanding the effect of crosslink structures on the physical properties of cellulose. It has been hypothesized

* Corresponding author.
E-mail address: chenw@umbi.umd.edu (W. Chen).
[1] Present address: 9600 Gudelsky Drive, Rockville, MD 20850, USA.

0032-3861/$ - see front matter © 2003 Elsevier Ltd. All rights reserved.
doi:10.1016/j.polymer.2003.11.020

that traditional crosslinks are too rigid to allow cellulose chains to evenly distribute applied stress during deformation, thus resulting in loss of mechanical properties. One solution to this problem may be the use of an elastic crosslink, the structure of which is more flexible than the current rigid commercial crosslinks and is also easily extensible yet completely recoverable. Cellulose fabrics treated with such a durable-press finishing agent should have good care-free and wrinkle-resistant properties with minimum loss of mechanical strength. The objectives of this initial research phase were: (1) construct amorphous cellulose models whose predicted physical properties are consistent with those of amorphous cellulose; and (2) simulate the extension and recovery of amorphous cellulose, in order to develop a more fundamental understanding for the poor wrinkle recovery of cellulose fibers.

2. Experimental

The majority of the computational results obtained were generated using the program Cerius2™, developed by BIOSYM/Molecular Simulations (now Accelrys). A SGI O2, with a 270 MHz processor and 512 MB main memory, and a SGI OXYX2, with eight 400 MHz processors and 16.0 GB main memory, both operating under IRIX 6.5, were used for all calculations.

2.1. Model building

Cellobiose, which can be considered as the repeat unit for cellulose [9], was used to build the cellulose chains. The chemical structure for cellobiose is shown in Fig. 1.

Six models, each with one cellulose chain of 20 cellobiose repeat units or 843 atoms, were built and then relaxed by molecular mechanics. The amorphous cell building method proposed by Theodorou and Suter [11] was employed. The initial conformation of the cellulose chain in each model was generated using a Monte Carlo method and then packed into a $20 \times 20 \times 20$ Å^3 cubic cell. Periodic boundary conditions (PBC) were used in all amorphous cellulose model building. With PBC, a molecular system is constructed to have the same density as that of the real system and then repeated through space, such that the real system can be simulated by a molecular model with fewer atoms. Since each cell is surrounded by 26 cells, it is feasible to directly calculate inter-molecular interactions, which is the focus of this work. The cell size was chosen to be larger than the calculated persistence length of cellulose, 7.89 Å, as the movement of each segment influences itself, under PBC, through its self-replica [19,20]. An initial density of 1.40 g/cm^3 was used. Electrostatic interactions were explicitly considered by assignment of proper partial charges to individual atoms by the charge-equilibrium method of Rappe and Goddard [21], and the Ewald summation method [22] was employed for evaluation of the non-bonded interactions. The structure was then relaxed and optimized as follows. The amorphous cell was first minimized by molecular mechanics. It was then relaxed through NVT molecular dynamics for 40 ps at 1000 K. A minimum energy structure in the dynamics energy vs time evolution diagram was chosen and minimized. It was then subjected to 5 cycles of minimization and NPT molecular dynamics for 40 ps at 298 K. Finally, a full optimization for cell parameters and atomic coordinates was performed by molecular mechanics.

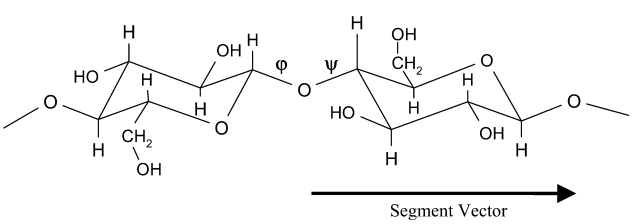

Fig. 1. The repeat unit for cellulose used is the cellobiose group, made up of two β-D-glucopyranose rings. The segment vector is defined by two glycosic linkage oxygen atoms.

The average cell densities as a function of temperature were determined using NPT dynamics. Models were relaxed at 200 K through NPT dynamics for 20 ps and the densities over the last 5 ps of the simulation were averaged. Using this method, average densities were calculated over a temperature range from 200 to 700 K, in 50 K increments.

2.2. Extension and recovery of cellulose models

The relaxed amorphous cellulose models were extended and then compressed in order to investigate their stress–strain properties. People have investigated this deformation behavior of amorphous polymers by two ways: molecular dynamics and molecular mechanics. Compared with molecular dynamics, molecular mechanics requires much less computing time without a significant loss of accuracy [23,24]. By molecular mechanics, strains are applied by changing the cell parameters. For example, in order to simulate the application of strain ε_{33} on the model, only the value of the cell parameter c is increased (or decreased) with all other cell parameters and atom coordinates fixed. Then with c fixed, all other cell parameters, as well as the atomic coordinates, are optimized by molecular mechanics. The stress, σ_{33}, is then obtained from the corresponding component of the internal stress tensor. Each amorphous cellulose model was extended using this method with a strain increment of 0.5% (roughly 0.1 Å on each amorphous cellulose cell) and a maximum strain of 30%, and the resultant stress was calculated as a function of strain.

Deformation recovery calculations were performed on all models in a similar way. The strained models were compressed back to 0% strain from four different strain positions: 2, 4, 10 and 15%, using a step size of 0.5% strain. Models were relaxed by molecular mechanics and the stress was obtained from the internal stress tensor at each step.

2.3. Model property calculations

The following properties were calculated in order to identify structural changes in cellulose models during extension.

2.3.1. Orientation function

The orientation function is defined as $\langle P_2 \rangle = [3\langle \cos^2\theta \rangle - 1]/2$, where θ is the angle between a segment vector and the direction in which the external stress is applied. A segment is defined as a glucose unit in the chain, and the vector is defined by the two glycosic linkage oxygen atoms, as shown in Fig. 1. The average orientation was determined over all unit vectors in the chain with respect to the direction along which extension was applied, and then averaged over three extension directions for one model, and then averaged over all six models.

2.3.2. Free volume

The free volume calculations were performed using Cerius2 based upon the work by Misra and Mattice, which provides a very complete analysis for these calculations [25]. The basic procedure consisted of four steps: (a) generate a three-dimensional grid (the increment used in this research is 0.4 Å) and impose it on the simulation cells; (b) assign the state of occupancy for each site in the grid. A site is defined as occupied if it is within the van der Waals radii of any atoms; (c) find the connectivity between the vacant sites and define free volume; (d) calculate the size of the free volume. PBC were imposed in the calculation.

2.3.3. Hydrogen bonds

Hydrogen bonds were identified based on geometrical considerations. A hydrogen bond was considered formed when the distance between a hydrogen atom and an oxygen atom was less than 3.0 Å and the angle between the proton acceptor, the proton and the proton donor was greater than 90°. Both inter-molecular and intra-molecular hydrogen bonds were taken into account. Inter-molecular hydrogen bonds are those formed between the hydroxyl groups of the parent chain and the hydroxyl groups of the image chains created by the PBC. Hydrogen bonds in all models were identified and their bond lengths were calculated from the coordinate data files. All hydrogen bond atom pairs were also identified and monitored in order to track the breaking and reforming of hydrogen bonds during both extension and compression of the models.

2.3.4. Potential energy and its components

The typical potential energy function can be written as:

$$E_{\text{tot}} = E_{\text{l}} + E_\theta + E_\omega + E_\chi + E_{\text{vdW}} + E_{\text{columbic}},$$

where E_{l} is a bond function that describes the potential energy change due to bond stretching, E_θ is a bond angle function, E_ω is a dihedral angle function, E_χ is an out-of-plane bend function, E_{vdW} is a van der Waals interaction function, and E_{columbic} is a Columbic interaction function. The change of each potential energy component reflects the change of its corresponding structure element. These were also evaluated during both extension and compression of the models.

3. Results and discussion

3.1. Characterization of amorphous cellulose models

Three force fields which have previously been used for crystal cellulose, Dreiding II [26], UNIVERSAL 1.02 [27], and pcff_300_1.01 [28,29,30], were evaluated based on final amorphous cellulose density obtained with each force field. The final model density was chosen as the evaluation criteria since its value is dependent upon both the packing of molecular chains in cells and the magnitude of interactions between molecular chains, and is further dependent upon the energy equations and parameter sets of these selected force fields. Average cell densities calculated using these force fields are presented in Table 1. Models generated using the pcff_300_1.01 force field had the highest density of the three force fields evaluated and had an average density closest to the reported literature value of 1.48 g/cm^3. Thus, this force field was used for all further calculations.

Six separate amorphous cellulose models were generated and relaxed according to the procedures outlined in Section 2.1. The average root mean square internal stress in these models was calculated to be 1.231 MPa, which is small when compared to the elastic constants such as Young's Modulus, 8.45 GPa [31] for viscose rayon, suggesting that these models were sufficiently relaxed and in an equilibrium state.

The basic requirement for these amorphous cellulose models in this work is that they are able to reflect the mechanic properties of real amorphous cellulose. The following properties were calculated based upon these models for the purpose of evaluation: solubility parameter, glass transition temperature, stiffness matrix, and radial distribution function (RDF).

The Hildebrand solubility parameter, δ, is defined as the square root of the cohesive energy density, E_{coh}/V, where V is the molar volume of an amorphous cell. The cohesive energy is a function of intermolecular interactions and is calculated as the difference in the potential energies between the isolated chain and the parent chain in the bulk,

$$E_{\text{coh}} = E_{\text{isolated}} - E_{\text{bulk}}.$$

Table 1
Average cell density calculated using different force fields

Force field	Dreiding II	UNIVERSAL 1.02	Pcff_300_1.01	Literature value [31]
Density (g/cm^3)	1.071 ± 0.072	1.213 ± 0.054	1.385 ± 0.032	1.48

The solubility parameter is written as

$$\delta = ((E_{\text{isolated}} - E_{\text{bulk}})/V)^{1/2}$$

$$= ((E_{\text{isolated}} - E_{\text{bulk}})\rho/M)^{1/2}$$

where ρ is the cell density and M is the molecular weight of the cellulose chain. Simulation values are listed in Table 2, where E_{isolated}, and E_{bulk} were the average potential energies over six models after energy minimization. The solubility parameters were calculated using an average model density of 1.385 g/cm^3 and a molecular weight (M) of 6503 for the cellulose chain consisting of 20 cellobiose units. The average solubility parameter was calculated to be 9.3 (cal/cm^3)$^{1/2}$, which is comparable to literature values [32] of 9–10 (cal/cm^3)$^{1/2}$ reported for rayon fibers.

The value for the glass transition temperature (T_g) is also a function of intermolecular interactions. Usually the greater the intermolecular attractions, the higher the glass transition temperature. A variety of material properties, such as specific volume and heat capacity, change significantly in the vicinity of the glass transition temperature. Thus, they are usually measured as a function of temperature to determine the T_g of a material. In this research, the average glass transition temperature for the amorphous cellulose models was calculated using the approach proposed by Rigby and Roe [33,34]. Fig. 2 is a plot of the average specific volume calculated for these models as a function of temperature. T_g was determined as the intersection of the regression fits. The linear portions of the plot intercept at roughly 500 K, yielding the T_g for cellulose models. This calculated T_g is close to the experimental value of 220–240 °C [32] reported for viscose rayon.

The stiffness matrix was calculated based upon the work of Fan and Suter, using a constant strain minimization method incorporated in the Cerius2 Mechanical Property Module. In the constant strain minimization procedure, small strains (0.05%) are applied to the periodic structure followed by minimization. The stiffness matrix is derived from the change in the resultant stress calculated as a function of applied strain. For an isotropic amorphous material, the stiffness matrix should be symmetric and have the following form [20]:

$$\begin{matrix} \lambda+2\mu & \lambda & \lambda & 0 & 0 & 0 \\ \lambda & \lambda+2\mu & \lambda & 0 & 0 & 0 \\ \lambda & \lambda & \lambda+2\mu & 0 & 0 & 0 \\ 0 & 0 & 0 & \mu & 0 & 0 \\ 0 & 0 & 0 & 0 & \mu & 0 \\ 0 & 0 & 0 & 0 & 0 & \mu \end{matrix}$$

where λ and μ are Lame's constants. The value for Young's modulus E, shear modulus G, bulk modulus B, and Poisson ratio ν are calculated from the Lame's constants as follows [20]:

$$E = \mu(3\lambda + 2\mu)/(\lambda + \mu) \qquad G = \mu$$

$$B = \lambda + 2\mu/3 \qquad \nu = \lambda/2(\lambda + \mu).$$

The average stiffness matrix calculated for the amorphous cellulose models is presented in Table 3. This calculated stiffness matrix is consistent with that for isotropic materials. Here, all elements that should be identical for an ideal isotropic material are similar. Those elements that should be zero for an ideal isotropic material are significantly smaller in comparison to the average Lame's constants. The values for Young's modulus, shear modulus, bulk modulus, and Poisson ratio, calculated from the

Table 2
Average solubility parameter of amorphous cellulose models from simulation

Average E_{bulk} (kcal/mol)	E_{isolated} (kcal/mol)	E_{coh} (kcal/mol)	δ (cal/cm^3)$^{1/2}$
53.181 ± 5.336	459.682 ± 3.891	406.501 ± 5.185	9.3 ± 1.1

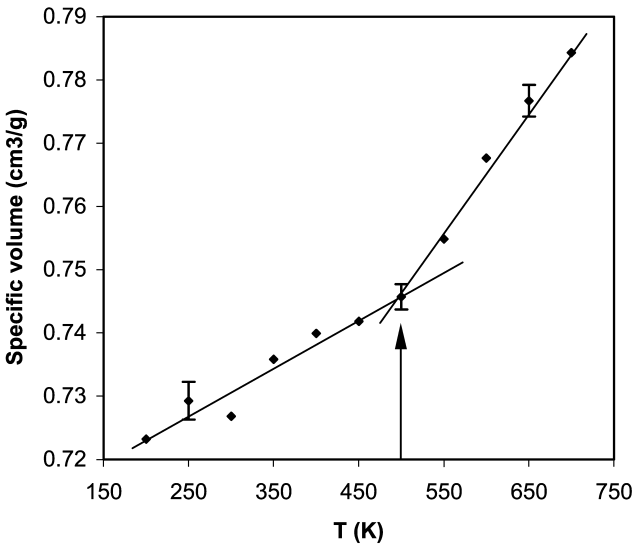

Fig. 2. Specific volume of amorphous cellulose models as a function of temperature. The standard deviations are presented at only 200, 500 and 650 K for clarity.

Table 3
Average stiffness matrix calculated for amorphous cellulose (GPa)

16.45 ± 1.78	8.54 ± 1.03	8.45 ± 1.17	−0.12 ± 0.21	−1.13 ± 0.46	0.19 ± 0.25
10.59 ± 1.21	15.80 ± 2.06	9.45 ± 1.06	−2.30 ± 0.85	1.99 ± 0.73	−0.24 ± 0.44
8.89 ± 0.85	8.75 ± 0.96	18.99 ± 2.55	−0.07 ± 0.19	−0.99 ± 0.58	0.14 ± 0.31
−0.31 ± 0.72	0.57 ± 1.01	0.95 ± 0.35	5.89 ± 0.69	0.10 ± 0.07	0.17 ± 0.09
−0.62 ± 0.52	0.62 ± 0.38	−0.42 ± 0.17	0.26 ± 0.15	5.82 ± 0.59	0.34 ± 0.13
0.52 ± 0.29	0.41 ± 0.92	0.09 ± 0.08	−0.15 ± 0.22	0.43 ± 0.26	6.16 ± 0.48

average Lame's constants, are presented in Table 4. The calculated value for Young's Modulus, 10.42 GPa, is slightly larger but comparable to the literature value for viscose rayon, 8.45 GPa [31].

The RDF was calculated for amorphous cellulose models, as well as for crystal models of cellulose I [9,31] and cellulose II [18,31], in order to identify any long-range order in the amorphous cellulose models. Crystal models were built based upon the parameters in the references. One fundamental difference between the crystalline and amorphous states is the existence of long-range order found only in the former. The RDFs for the crystal and amorphous cellulose models are presented in Fig. 3. The RDF for each model has four large peaks around 1.0–1.5 Å, which correspond to the C–H, O–H, C–C and C–O bond lengths, in addition to many smaller peaks between 2.0 and 3.0 Å which include the hydrogen bonding atom distances. For cellulose I and cellulose II, there are some relatively large peaks observed at distances larger than 3.0 Å. These peaks are due to the periodic repeating of structural units and can thus be considered as an evidence of long-range order. For example, the peaks around 5.5 Å, which appear in the RDFs for cellulose I and cellulose II, correspond to the distance between the glycosic linkage oxygen atoms. On the curve for the amorphous cellulose models, there are no peaks observed beyond 3.0 Å. Compared with the RDFs for cellulose I and cellulose II, the RDF for the amorphous cellulose models shows no long range order. Moreover, as mentioned above, the calculated value for Young's Modulus is comparable to the value measured for viscose rayon, whose mechanical properties are governed by its amorphous character.

Based upon the above results, it can be concluded that these amorphous cellulose models are representative of the amorphous structure in cellulose as far as mechanic properties are concerned.

3.2. Deformation and recovery in cellulose

Fig. 4 is a plot of the average stress calculated as a function of applied strain from 18 data sets (6 models in 3 extension directions). It is similar in appearance to the stress–strain curve obtained for viscose rayon [35]. A linear relationship between stress and strain is observed at low strain, which corresponds to elastic deformation. At higher strain the curve gradually levels off indicating a yielding behavior. A yield strain of approximately 7–8% is observed, which is close to that observed for viscose rayon. Moreover, the average initial modulus calculated from this stress–strain data set is 10.3 GPa, which is comparable with the literature value for viscose rayon [1] and with that calculated from Lame's constants and presented in Table 4.

Recovery calculations were performed using molecular mechanics in order to examine the recovery of amorphous cellulose models from the applied strain. The strained models were compressed back to 0% strain in 0.5% strain decrements from four different initial strain positions: 2, 4, 10 and 15%. Models were relaxed by molecular mechanics and the stress obtained from the internal stress tensor at each step. Fig. 5 is a plot of the stress during extension and compression as a function of strain. The models compressed from an initial strain of 2% showed essentially complete recovery. From 4% strain, the models did show a small yet permanent deformation. This result is comparable with experimental results in that the recovery of cellulose fibers from stress–strain measurements is moderate, and even small strains result in permanent deformation [36]. For extensions exceeding the yielding point, larger permanent deformations are observed. These results are consistent with the fact that non-crosslinked cellulose has poor recovery from deformation.

3.3. Yielding in amorphous cellulose models

As presented in Fig. 4, these cellulose models show an apparent yielding point at approximately 7–8% strain. In

Table 4
Mechanical properties of amorphous cellulose models (experimental value [31] for Young's modulus is in parenthesis)

Young's modulus (GPa)	Bulk modulus (GPa)	Compressibility (GPa)	Shear modulus (GPa)	Poisson's ratio
10.42 ± 1.08 (8.45)	13.258 ± 1.731	0.0754 ± 0.0094	5.955 ± 0.673	0.232 ± 0.0313

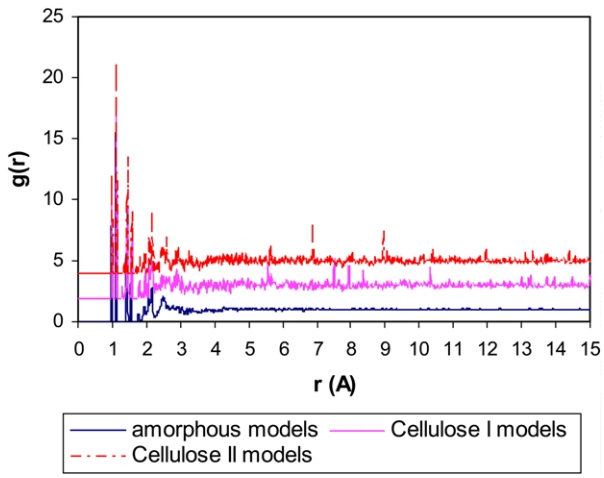

Fig. 3. Radial distribution function for amorphous cellulose, cellulose I and cellulose II crystal models. RDF for cellulose I models is shifted 2 units upward and RDF for cellulose II models is shifted 4 units.

order to clarify the mechanism for yielding and poor recovery from deformation, the structural elements of these cellulose models were examined as a function of extension.

The effect of applied strain on the segmental orientation function $\langle P_2 \rangle$ was calculated. The average value for $\langle P_2 \rangle$ prior to deformation was zero, indicating a completely random orientation for the initial structure. As the strain was increased, the value of $\langle P_2 \rangle$ increased slightly, reaching a value of 0.06 at 15% strain. Thus, extension of the models did not significantly change the orientation of chain segments.

The end-to-end distance and radius of gyration were calculated to check for changes in chain dimensions. The initial end-to-end distance and the radius of gyration were 54.2 and 23.2 Å, respectively. With the increase in strain, both end-to-end distance and radius of gyration increased almost linearly. However, the changes were relatively small: at 15% strain, the end-to-end distance increased by

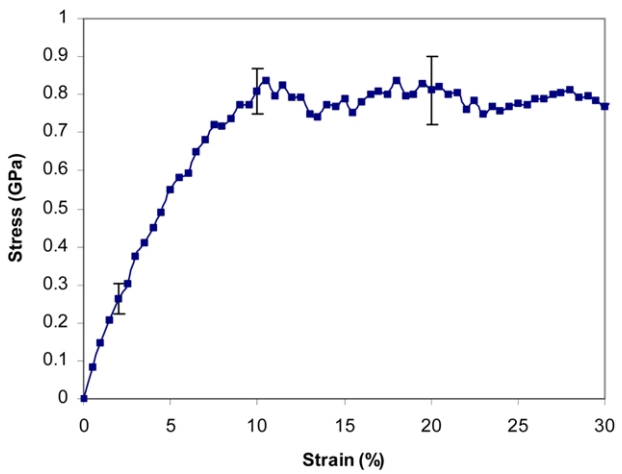

Fig. 4. Average stress–strain curve calculated for amorphous cellulose models. Standard deviations are presented at only 2, 10 and 20% strain for clarity.

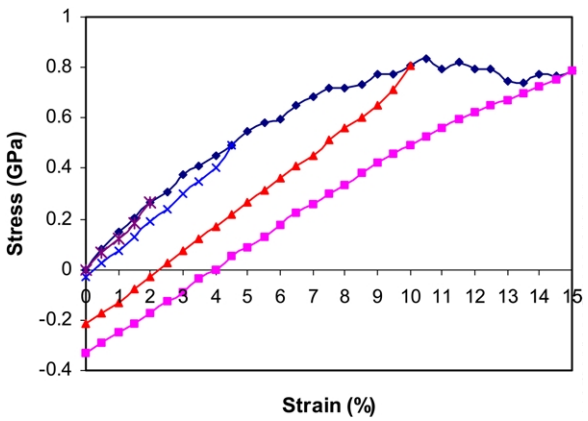

Fig. 5. Calculated stress due to applied strain for extension and compression from 2, 4, 10 and 15% strain, respectively.

3.3% and radius of gyration increased by 2.9%. Thus, deformation to 15% strain did not significantly change the chain dimensions.

The φ, ψ-torsion angle distributions were calculated to identify any conformation transitions which may have occurred during extension. The torsion angles φ and ψ are defined in Fig. 1. The initial torsion angle distribution was calculated over six models, and the distribution at 15% strain was calculated for each of the eighteen models produced by extension. Compared with the torsion angle distribution prior to deformation, the distribution at 15% strain was only slightly broader. Examination of each individual torsion angle showed that no angle changed more than 8°. Thus, extending the amorphous cellulose models to 15% strain did not induce any conformation transitions.

The RDF of amorphous cellulose models at 15% strain was calculated and compared with that for the amorphous cellulose cell prior to deformation. The peak positions in the range of $r < 2$ Å, which are due to the atomic connectivity in the repeating units and reflect covalent bond lengths, did not change during extension indicating that the covalent bond lengths remained unchanged, as expected. Interestingly, those peaks from 2 to 3 Å which include the hydrogen bond distances were observed to shift to slightly larger values.

The cell volume and free volume of the amorphous cellulose models were calculated as a function of strain and these results are presented in Fig. 6. At 15% strain the cell volume increased by 6.4%, whereas the free volume showed a significant increase of 21.5%. The free volume was calculated as the difference between the cell volume and the volume occupied by the cellulose chain itself. This latter calculation is based upon the van der Waals radii of the atoms. Therefore, this large increase in free volume could only be due to an increase in separation between chain segments, disrupting the secondary bonding between chain segments, i.e. the hydrogen bonds.

Fig. 7 is a plot of the average percent elongation of hydrogen bonds between cellulose chain segments as a function of strain. At small strains a linear relationship

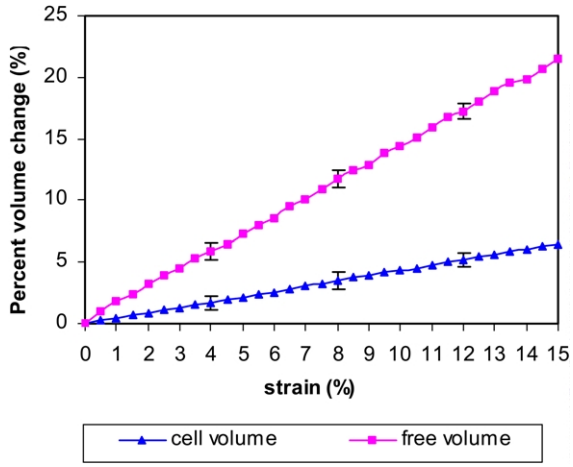

Fig. 6. Relative change of cell volume and free volume with strain. Standard deviations are presented at only 4, 8 and 12% strain for clarity.

between the hydrogen bond percent elongation and strain is observed, indicating that hydrogen bonds take up the strain in the cellulose models. Interestingly, the average percent elongation decreased at 6–7% strain which is close to the yielding strain observed from the calculated stress–strain data presented in Fig. 4. The decrease in percent elongation is attributed to the breaking of hydrogen bonds. The calculated percent elongation is lowered when highly strained hydrogen bonds, which have longer bond lengths, break and are no longer considered as hydrogen bonds in this calculation. Thus, the yielding behavior in amorphous cellulose models is directly related to the breaking of hydrogen bonds.

Fig. 8 is a plot of the change in potential energy, and its components, as a function of applied strain. The potential energy components reflect the change in structural elements such as bond lengths, bond angles, torsion angles, and non-bonded chain segments during deformation. In this figure, 'bonded' refers to the energy terms corresponding to the changes in bond lengths, bond angles and torsion angles. The

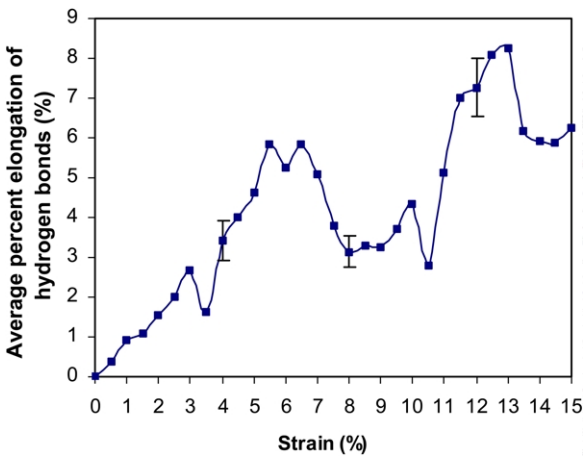

Fig. 7. The percentage of the hydrogen bond elongation with strain for amorphous cellulose models. Standard deviations are presented at only 4, 8 and 12% strain for clarity.

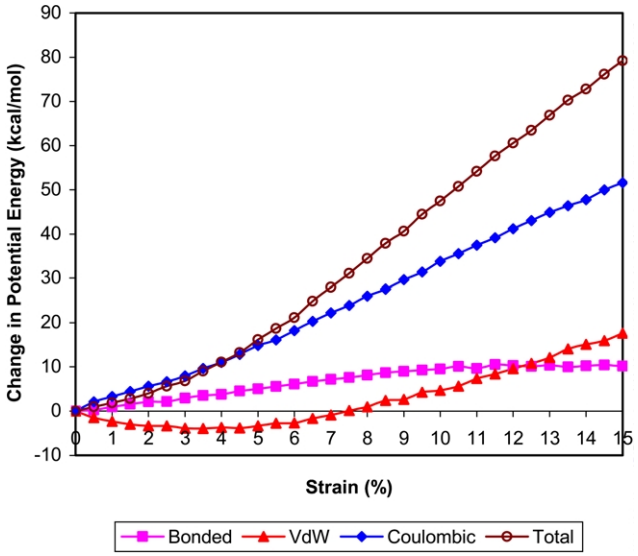

Fig. 8. Strain energy and its components with strain for amorphous cellulose models.

slope of the curve for the total potential energy increases with strain up to about 6% strain, beyond which the potential energy varies linearly with strain. The applied strain on the models influenced each of the energy components differently. The effect on the 'bonded' energy terms is small. This is in agreement with the previous RDF and torsion angle distribution results in that the covalent bond lengths and torsion angles did not change significantly during deformation. The van der Waals (vdW) term remained essentially unchanged up to 8% strain, beyond which it increased slightly. The small decrease in the vdW term at small strain is believed to be due to the release of residual internal stress due to the breaking of hydrogen bonds. The overall change in potential energy due to the applied strain is dominated by changes in the Columbic term. The pcff_300_1.01 force field does not have a specific hydrogen bond term; instead the energy due to hydrogen bonding interactions is calculated within the Columbic term. To determine whether the hydrogen bonding or partial charges or both, reflected in the Columbic term, dominates the strain energy change, six amorphous models of fully methylated cellulose with an initial density of 1.40 g/cm^3 were built and deformed. The changes of strain energy and its components were also calculated for the fully methylated cellulose models. Instead of the Columbic term, it is the van der Waals term that dominates the strain energy change in these modified cellulose models. If it is assumed that methylated cellulose has a similar chemical environment as cellulose except the absence of hydrogen bonds in the former, it can be concluded that the contribution from hydrogen bonding dominates the Columbic energy of cellulose models. Therefore, these energy calculation results are consistent with the earlier results, that is, the hydrogen bonds take up the applied strain and the yielding behavior of amorphous cellulose models is due to the breaking of hydrogen bonds.

All hydrogen bond atom pairs were monitored during extension of models. Our calculation results showed that among the broken hydrogen bonds during extension, inter-molecular ones accounted for more than 90%. Such a large percentage suggests that large chain movements occurred and each chain tended to move as a unit. Before further discussion about the behavior of inter-molecular hydrogen bonds during extension, it is necessary to define the number of original hydrogen bonds broken, which is shown in Fig. 9. In this illustration, each hydrogen bond is identified according to the specific atoms participating in that hydrogen bond. Of the three original hydrogen bonds prior to deformation (H1–O4, H2–O3 and H3–O2), only one remains (H3–O2) and one new hydrogen bond is formed (H1–O3) after deformation. The number of original hydrogen bonds broken is thus equal to 2.

The change in number of original hydrogen bonds as a function of strain is presented in Fig. 10. As strain is increased, the total number of inter-molecular hydrogen bonds was found to decrease. Even at strains below the observed yielding point, the inter-molecular hydrogen bonds were being broken. This is consistent with the recovery data (Fig. 5) which showed that even a small strain (4%) can result in permanent deformation in cellulose models. A much greater decrease in the number of hydrogen bonds is observed at strains larger than 6%. The change in the total number of hydrogen bonds as a function of strain is also presented in Fig. 10. The difference between these two curves at the same strain reflects the number of newly formed hydrogen bonds. Prior to the yielding strain, these two curves overlap, indicating that no new hydrogen bonds were formed. The number of new hydrogen bonds formed increases slightly from 6 to 11% strain where the largest decrease in the total number of hydrogen bonds was observed. This is consistent with the previous results (Fig. 7) in that the average hydrogen bond length dropped at 6–7% strain due to the breaking of hydrogen bonds. Interestingly, above 11% strain the decrease in total number of hydrogen bonds is nearly zero while the number of original hydrogen bonds still decreases with strain. One would expect the same number of new inter-molecular hydrogen bonds to be formed when some old ones are broken, if chains just slip past one another. If chains are just

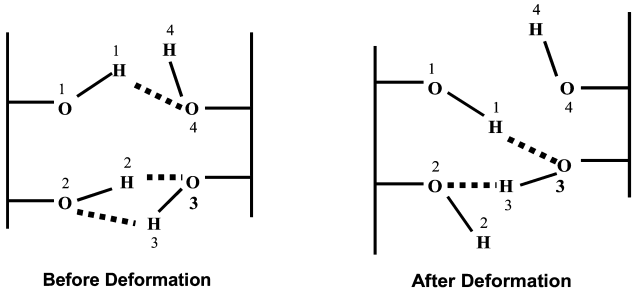

Fig. 9. Illustration of the number of original hydrogen bonds broken in cellulose.

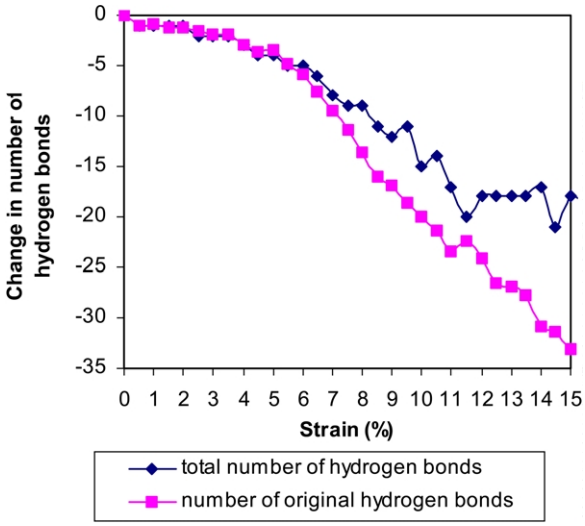

Fig. 10. Change in number of hydrogen bonds with strain when amorphous cellulose models were extended from 0 to 15% strain.

separated, it is unlikely that new hydrogen bonds would be formed and the total number of hydrogen bonds would keep decreasing with strain. Therefore, the results presented in Fig. 10 can be taken as an evidence of chain slippage.

Hydrogen bonds atom pairs were again tracked during compression of cellulose cells from 15% back to 0%. Fig. 11 is a plot of both the percentage of the original hydrogen bonds restored and the percentage of newly formed hydrogen bonds which were broken due to compression as a function of strain. As the cells were being compressed, the new hydrogen bonds which had been formed due to extension were being broken and the original hydrogen bonds which had been broken during extension were being restored. Referring back to Fig. 5, a 4% permanent deformation was observed when the models were extended to 15% strain and then compressed. The percentages of original hydrogen bonds restored and new hydrogen bonds

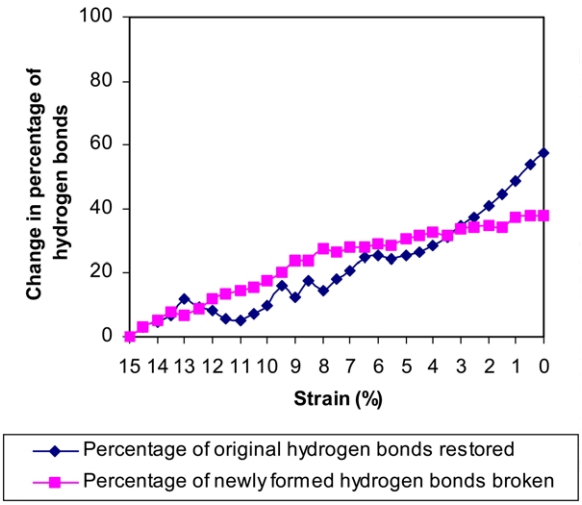

Fig. 11. Change in percentage of hydrogen bonds with strain when amorphous cellulose models were compressed from 15 to 0% strain.

broken are both approximately 30% at 4% strain. In other words, more than 2/3 of these new hydrogen bonds formed during extension remain intact after compression. It is thus the formation of these new hydrogen bonds which is responsible for the poor recovery of cellulose. These results support the traditional explanation for wrinkling, that is, hydrogen bonds formed in deformation prevent complete recovery.

4. Conclusions

Amorphous cellulose models were successfully generated with the use of pcff_300_1.01 force field. Properties related to inter-molecular interactions such as density, solubility parameter, T_g and selected mechanical properties were calculated and found to be comparable with literature values. The models were deformed using a successive straining procedure. The resultant stress–strain relationship was similar in appearance to that obtained from mechanical testing of real cellulosic materials, including a yielding at 7–8% strain.

The atomic structures of the models were evaluated over the entire range of applied strain. The average length of the intermolecular hydrogen bonds was found to drop at 6–7% strain, which is close to the yielding strain. This drop in average hydrogen bond length was found to be due to the breaking of highly strained hydrogen bonds. Moreover, the increase in potential energy was found to be mainly due to the decrease of hydrogen bond interactions. Therefore, it can be concluded that the observed yielding is due to the disruption of hydrogen bonds. Chain slippage occurred in extension as evidenced by breaking of original and formation of new hydrogen bonds. Only 1/3 of these new hydrogen bonds were broken during compression. The hydrogen bonds formed in extension tended to hold cellulose chain segments in new positions, thus resulting in poor recovery.

Thus, molecular modeling has provided insights into the mechanisms for the yielding and poor recovery of cellulose. In the next phase of this work, the effect of crosslinking reagents on the properties of amorphous cellulose will be examined in order to clarify the mechanism of strength loss due to crosslinking in cellulose fibers.

Acknowledgements

This work was supported by National Textile Center (NTC). The authors would like to thank the Center for Advanced Engineering Fibers and Films (CAEFF) for the use of their computational facility, in addition to Dr Michael Drews and Dr Steven Stuart for their valuable suggestions.

References

[1] Stevens CV, Smith BF. Text Res J 1970;40:749–60.
[2] Stam PB, Poon GSY, Spangler MJ. Text Res J 1956;26:960–5.
[3] Steiger FH, Wany SY, Hurwitz MD. Text Res J 1961;31:327–39.
[4] Nickerson RF. Am Dyestuff Reptr 1950;39:46–50.
[5] Smith AR. Text Res J 1956;26:836–51.
[6] Haydel CH, Janssen HJ, Seal JF, Gastrock EA. Text Res J 1957;27:975–82.
[7] Kamogawa H, Murase R, Sekiya T. Text Res J 1960;30:774–81.
[8] Nowakowski A. Text Res J 1951;21:740–6.
[9] Pizzi A, Eaton NJ. Macromol Sci—Chem 1985;A22(2):139–60.
[10] Marhofer RJ, Reiling S, Brickmann. J Phys Chem 1996;100(8):1350–4.
[11] Theodorou DN, Suter UW. Macromolecules 1985;18:1467.
[12] Ganster J, Blackwell. J Mol Model 1996;2:278–85.
[13] Rigby D, Roe RJ. J Chem Phys 1987;87:7285.
[14] Jin WK, Kyoungsei C, Won HJ, Hsu SL. Polymer 1998;39(26):7079–87.
[15] Fan CF, Hsu SL. Macromolecules 1992;25:266–75.
[16] Ogura I, Yamamoto T. Polymer 1995;36:1375–96.
[17] Fan CF. Macromolecules 1995;28:5215–26.
[18] Kolpak FJ, Blackwell J. Macromolecules 1976;9(2):273–8.
[19] Flory PJ. Statistical mechanics of chain molecules. New York: Wiley; 1969.
[20] Kaufman HS. Introduction to polymer science and technology: an SPE textbook. New York: Wiley; 1977.
[21] Rappe AK, Goddard III WA. J Phys Chem 1991;95:3358–63.
[22] Forcefield-Based Simulations, MSI, April 1997.
[23] Fan CF, Hsu SL. Macromolecules 1991;24:6244–9.
[24] Fan CF, Cagin T, Chen ZM, Smith KA. Macromolecules 1994;27:2383–91.
[25] Misra S, Mattice WL. Macrocolecules 1993;26:7274.
[26] Mckechnie JI, Haward RN, Brown D, Clarke JHR. Macromolecules 1992;26:198–215.
[27] Mayo SL, Olafson BD, Goddard III WA. J Phys Chem 1990;94:8897–911.
[28] Sun H, Mumby SJ, Maple JR, Hagler AT. J Am Chem Soc 1994;116:2978–3012.
[29] Sun H. Macromolecules 1996;28:701–21.
[30] Sun H. Macromolecules 1994;26:5924–38.
[31] Mark HF. Encyclopedia of polymer science and technology—plastics, resins, rubbers, fibers, vol. 3, New York: Wiley, 1982.
[32] Brandrup J, Immergut EH, Grulke EA. Polymer handbook, 4th ed. New York: Wiley; 1999.
[33] Rigby D, Roe RJ. Macromolecules 1989;22:2259.
[34] Rigby D, Roe RJ. Macromolecules 1990;23:5312.
[35] Morton WE, Hearle JWS. Physical properties of textile fibers. New York: Wiley; 1970.
[36] Steele R, Giddings LE. Text Res J 1956;26:116–23.